Astron. Astrophys. 323, 5–13 (1997)

ASTRONOMY
AND
ASTROPHYSICS

# Balmer emission-line profile variations in NGC 4593

**W. Kollatschny**[1] **and M. Dietrich**[2]

[1] Universitäts-Sternwarte Göttingen, Geismarlandstraße 11, D-37083 Göttingen, Germany
[2] Landessternwarte Heidelberg, Königstuhl, D-69117 Heidelberg, Germany,

Received 26 March 1996 / Accepted 9 August 1996

**Abstract.** We present results of a variability campaign of Balmer line profiles in NGC 4593. The continuum and the broad emission line intensities varied up to 50 per cent during the observing period. The rms profiles of the Balmer lines as well as the difference line profiles can be described by a limited number of strong components only: a central component and two to four outer components which are located more or less symmetrically with respect to $v_{rel}$ = 0 km $s^{-1}$. The components varied neither simultaneously nor with the same amplitude. But there is a trend that the pairwise components varied in a similar way. The outer line wings responded nearly simultaneously within of 2 days to continuum variations. The inner regions of the line profiles responded within about 5 days. Strong radial motions can be excluded to be dominant in the BLR. Indications have been found for the appearance or disappearance of line profile components within a few days only. The BLR seems to be clumpy and to consist of a limited number of clouds or cloud complexes only. These clouds or the ionizing source might have a bidimensional structure.

**Key words:** galaxies: individual: NGC4593 – galaxies: Seyfert – lines: profiles

## 1. Introduction

Most Seyfert 1 galaxies are variable in the optical on time scales of weeks to years. The study of the variable ionizing continuum and of the integrated line intensities can give us information on the structure of the broad line region (BLR) where these lines originate. Profile variations in Seyfert galaxies have been investigated so far only for a few objects due to observational limitations (e.g. Peterson 1987; Stirpe et al. 1988; Zheng et al. 1995; Wanders & Peterson 1996, Kollatschny & Dietrich 1996) while theoretical studies are available for more than 20 years (Blumenthal & Mathews 1975; Blandford & McKee 1982; Carroll & Kwan 1985; Robinson & Pérez 1990; Welsh & Horne 1991).

*Send offprint requests to*: W. Kollatschny

In this paper we present an analysis of a five months line profile variability campaign of NGC 4593 based on spectra taken in 1990. NGC 4593 is a nearby Seyfert 1 galaxy (z=0.0084) of Hubble type SBb with an apparent magnitude of $m_v$ = 13.2. It is a low luminous Seyfert 1 galaxy regarding the absolute magnitude $M_V = -20.5$ ($H_\circ$ = 50 km $s^{-1}$ $Mpc^{-1}$). NGC 4593 is a member of a group of 5 galaxies (Kollatschny & Fricke 1989). NGC 4593 was one of the key objects of a monitoring campaign (Lovers of Active Galaxies: LAG) of six Seyfert galaxies and two quasars. Typically once per week high signal to noise spectra were taken at the Canary Islands Observatories during the first half of 1990. A review of the campaign is given by Robinson (1995).

First results of the continuum variations and of the integrated H$\alpha$ and H$\beta$ variations in NGC 4593 have been published by Dietrich et al. (1994, hereafter Paper I) and Kollatschny & Dietrich (1993). NGC 4593 has gone through strong variations on short time scales during the observing period. Cross-correlating the line intensities with the optical continuum flux yielded a lag of four days indicating a very compact broad line region (BLR) in this active galaxy (Paper I). Santos-Lleó et al. (1994) presented results of an independent multiwavelength monitoring campaign of NGC 4593 from the near-IR to X-rays in 1985. They detected strong and rapid variations in all wave bands, too. In the following paper we discuss in detail line profile variations in NGC 4593. The study of the emission line profiles and their variation provides us with information on the structure and distribution of the broad line region emissivity as well as on the kinematics of the line emitting gas.

## 2. Observations and data analysis

H$\alpha$ and H$\beta$ spectra of the Seyfert galaxy NGC 4593 were observed as part of an international monitoring campaign at La Palma, Spain. These spectra were taken at the 4.2 m William Herschel Telescope (WHT) and the 2.5 m Isaac Newton Telescope (INT). H$\alpha$ spectra ($\lambda\lambda$:6200 — 7200Å) were obtained at 23 epochs and H$\beta$ spectra ($\lambda\lambda$:4500 — 5400Å) were obtained at 11 epochs from Jan. 2nd until June 6th, 1990. The individual observing dates as well as the observing conditions are published in Paper I.

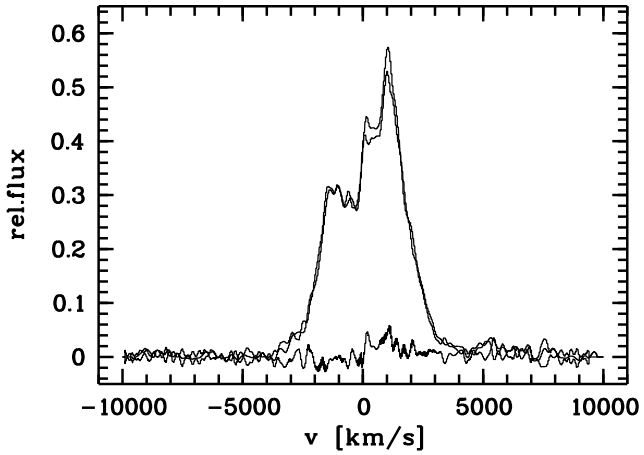


**Fig. 1.** Difference profiles of H$\alpha$ taken with the 4.2m and 2.5m telescopes during the same night (JD2447911) within two hours. The profiles have been computed with respect to the minimum state of the observing campaign. The difference of these two spectra is plotted at the bottom.

For a detailed investigation of line profile variations it is important that the spectra are obtained under homogeneous conditions. Therefore, it is of great advantage for our present study that only two telescopes and two spectrographs were used with fixed instrumental settings. In Fig. 1 H$\alpha$ difference profiles are plotted to show the influence of the different instrumentations. Given are difference profiles with respect to the minimum state of this campaign (JD = 2447968) for demonstrating small scale deviations in greater detail. The spectra were taken during the same night (JD=2447911) within two hours but at the WHT and INT telescopes with different spectrographs and different spectral resolution (0.73Å/pxl and 1.45Å/pxl). The difference spectrum at the bottom represents the uncertainty in the line profiles due to instrumental effects. The shape, the structure as well as the existence of substructures are identical in the profiles. The noise in the spectra is of the order of 1 per cent. At the positions of the narrow line components additional errors of 3 % in relative flux can be detected.

A very high signal to noise ratio is important for a detailed line profile analysis. Therefore, we selected only those spectra having a high signal to noise ratio ($>$ 20). For the final profile analysis we used high quality H$\alpha$ spectra obtained at 21 epochs. In Table 1 the Julian date and the measured intensities of seven line segments are given. The reason for the dividing of the profiles in seven segments (line core and three wing segments respectively) will be discussed in Sect. 3. H$\beta$ spectra were used only to determine mean and rms spectra.

The reduction procedure of the spectra has been described in detail in Paper I. The broad emission line intensities and their profiles were calibrated with respect to the narrow emission lines. We made the assumption that the intensity of the narrow emission lines is constant over time scales of years. This is plausible because they originate in a spatially more extended narrow line region. Furthermore, we tested on narrow band direct images that the narrow lines originate in regions smaller than one arcsec projected on the sky (priv.com. Pérez 1993). Therefore, possible guiding errors or a possible influence of different seeing conditions are negligible with regard to our relative calibration.

**Table 1.** Observed H$\alpha$ line segment intensities. The intensities of the segments are given in units of $10^{-14}$ erg s$^{-1}$ cm$^{-2}$. (Errors: 1 per cent in core segment, 5 per cent in outer wings.) Extent of the segments: -5000 — -2500 km s$^{-1}$ (outer blue wing) , -2500 — -1500 km s$^{-1}$ (middle blue wing) , -1500 — -500 km s$^{-1}$ (inner blue wing), -500 — +500 km s$^{-1}$ (core), +500 — +1500 km s$^{-1}$ (inner red wing) , +1500 — +2500 km s$^{-1}$ (middle red wing), +2500 — +5000 km s$^{-1}$ (outer red wing).

| Jul.date (2440000+) | out-blue (2) | mid-blue (3) | in-blue (4) | core (5) | in-red (6) | mid-red (7) | out-red (8) |
|---|---|---|---|---|---|---|---|
| 7894.730 | 31.4 | 47.5 | 82.3 | 110.1 | 103.3 | 40.8 | 25.5 |
| 7897.685 | 34.0 | 48.2 | 84.1 | 113.0 | 103.3 | 42.1 | 28.2 |
| 7902.644 | 31.8 | 46.0 | 80.5 | 108.5 | 96.2 | 41.5 | 25.4 |
| 7911.707 | 28.3 | 43.6 | 76.1 | 98.6 | 93.0 | 40.6 | 24.4 |
| 7916.721 | 22.6 | 34.1 | 60.2 | 78.3 | 71.9 | 27.1 | 18.2 |
| 7920.735 | 26.0 | 36.9 | 65.4 | 91.2 | 80.6 | 30.2 | 21.9 |
| 7923.681 | 27.6 | 39.9 | 70.9 | 101.0 | 85.6 | 33.0 | 24.5 |
| 7928.688 | 27.6 | 35.8 | 60.9 | 85.0 | 73.4 | 30.8 | 22.0 |
| 7931.654 | 28.4 | 39.0 | 65.2 | 87.2 | 72.5 | 30.9 | 22.5 |
| 7939.625 | 27.1 | 39.1 | 66.2 | 85.1 | 72.3 | 27.4 | 19.3 |
| 7944.666 | 26.9 | 37.9 | 64.5 | 86.7 | 75.0 | 29.4 | 21.5 |
| 7957.554 | 23.4 | 31.0 | 54.1 | 75.6 | 63.2 | 23.2 | 18.6 |
| 7968.653 | 25.5 | 31.8 | 52.1 | 70.0 | 55.9 | 21.7 | 18.3 |
| 7984.508 | 31.2 | 43.0 | 70.9 | 94.0 | 79.5 | 31.5 | 23.1 |
| 7997.500 | 28.3 | 36.8 | 60.9 | 86.4 | 69.6 | 26.2 | 20.3 |
| 8014.463 | 33.3 | 41.3 | 67.9 | 90.3 | 76.1 | 30.7 | 23.7 |
| 8025.490 | 28.5 | 32.6 | 57.2 | 81.4 | 65.6 | 24.1 | 20.2 |
| 8027.581 | 31.8 | 36.2 | 61.8 | 85.6 | 68.7 | 25.8 | 21.3 |
| 8031.639 | 32.0 | 35.2 | 59.3 | 80.6 | 64.1 | 26.6 | 22.7 |
| 8036.543 | 30.6 | 34.4 | 57.2 | 78.2 | 62.5 | 25.1 | 21.2 |
| 8049.495 | 29.2 | 32.8 | 56.4 | 79.5 | 66.7 | 26.4 | 22.7 |

Small scale shifts of less than 1 Å in wavelength scale have been corrected with respect to the narrow lines. We rebinned our spectra having resolutions of 0.73 Å and 1.45 Å respectively to a uniform step size of 1 Å. Thereafter we smoothed the profiles with a narrow Gaussian filter of 3 Å FWHM. Although the high frequency noise was redistributed the overall shape of the emission line profile remained unchanged.

The H$\alpha$ and H$\beta$ spectra have been corrected for redshift (z = 0.0084) and transformed into velocity space for better comparison of the profiles. The redshift of z = 0.0084 has been determined from the narrow emission lines.

For the detailed determination of small scale profile variations we decided to study difference line profiles with respect to the minimum state and between two adjacent epochs. Generally, one could use other spectra than the minimum profile as reference e.g. the mean profile. Therefore, we made some tests whether the selection of a certain reference spectrum (mean profile, smoothed minimum profile etc.) introduces artificial features. We found no influence of the existence of individual line components on the reference spectrum. We decided to use the minimum H$\alpha$ spectrum as reference profile for considering

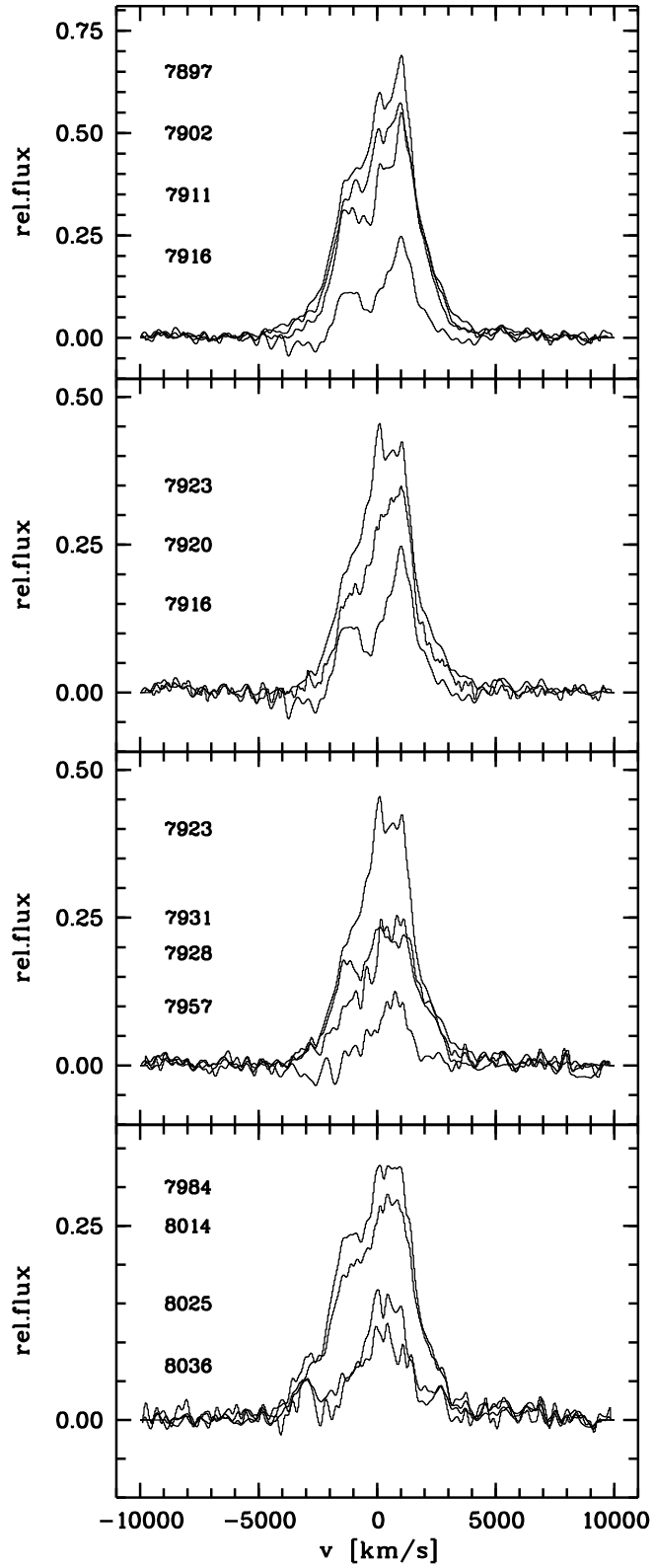


**Fig. 2.** Difference profiles of H$\alpha$ with respect to the minimum spectrum transformed into velocity space: On top the first decreasing period is plotted; in the upper middle panel the adjacent increasing period is given. The lower middle panel shows the evolution of the line profile towards the minimum state; profile variations during the second half of the monitoring campaign are presented in the bottom panel.

emission line profiles only. From the outer sections of the difference spectra (Fig. 2) one can estimate that the errors in relative flux are of the order of two to five per cent. Additional errors could be introduced in the difference profiles at the places of the narrow line components due to still existing small scale errors in wavelength scale and due to different spectral resolution. These errors are expected to be at the wavelength positions of the narrow [NII] and H$\alpha$ lines at $v_{rel} = -675,\ 0,\ 940$ km s$^{-1}$.

## 3. Results

For studying the line profile structures we calculated mean and rms spectra of H$\alpha$ and H$\beta$ first. Furthermore, light curves of the integrated H$\alpha$ line and of individual line segments have been constructed. We determined difference spectra with respect to the minimum H$\alpha$ profile of our observing period as well as difference spectra between subsequent epochs to look for variations of individual line components.

Finally, we determined the cross-correlation functions (ICCFs) of line segments with respect to the ionizing continuum to investigate the velocity structure within the BLR.

### *3.1. Mean and rms spectra*

A mean H$\alpha$ profile has been calculated by using all our spectra except that one taken at JD...7995. This spectrum has been discarded because of its low signal to noise ratio in comparison to the other spectra (cf. Fig. 1, Paper I). The rms profile of H$\alpha$ has been constructed by using the same spectra. The mean and rms H$\alpha$ spectra are shown in Fig. 3. The mean H$\alpha$ profile has been normalized to the maximum intensity of the broad H$\alpha$ line component. The H$\alpha$ rms profile has been scaled to the same intensity for better comparison of the line profiles. Differences in their profiles are evident. The H$\alpha$ rms profile is steeper than the mean profile. Both profiles are comparable regarding their FWHM (3400 $\pm$ 200 km s$^{-1}$) but the width at the bottom of the mean profile (FWZI) amounts to 18000 $\pm$ 1000 km s$^{-1}$ instead of 9000 $\pm$ 1000 km s$^{-1}$ (rms spectrum). Furthermore, the mean spectrum is more asymmetric due to the strong blue wing. If one makes the assumption that the rms profile should be smooth and symmetric about its peak one can distinguish three components (cf. Fig. 3), i.e. a red component centered at $v_{rel}$ = 1000 $\pm$ 100 km s$^{-1}$, a central component at 80 $\pm$ 50 km s$^{-1}$, and a blue component at -1000 $\pm$ 100 km s$^{-1}$. The red component is evidently stronger than the blue component. There might be a second blue component at -1300 $\pm$ 100 km s$^{-1}$. The central component seems to be steeper in comparison to the outer components. Mean and rms profiles of H$\beta$ have been calculated from all available spectra. The normalized profiles are plotted in Fig. 4. Again the rms profile is steeper than the mean profile. Although the signal to noise ratio is not as high as that for H$\alpha$ three components can be detected too in the rms spectrum: a red component at 1150 $\pm$ 200 km s$^{-1}$, a central component at 150 $\pm$ 200 km s$^{-1}$, and a blue component at -1150 $\pm$ 200 km s$^{-1}$. The outer H$\beta$ components are broader in comparison to the steep central component too. Following

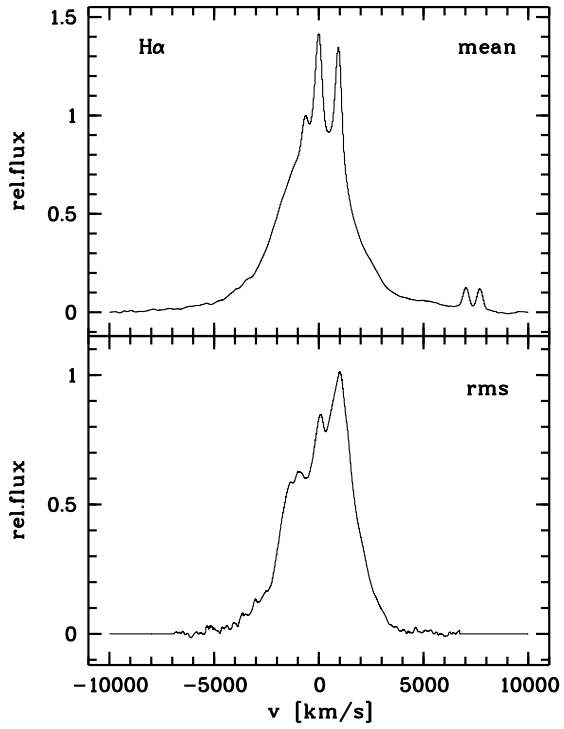


**Fig. 3.** Mean and rms profiles of H$\alpha$.

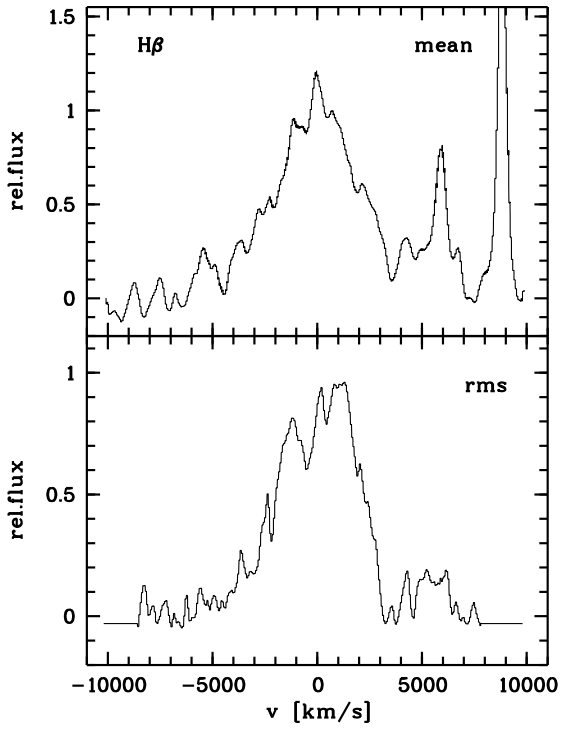


**Fig. 4.** Mean and rms profiles of H$\beta$.

trends can be seen when comparing the mean and rms-profiles of H$\alpha$ with those of H$\beta$. The H$\beta$ lines are broader by 10 - 20 per cent. But the basic structure of the rms-profiles is similar. Both Balmer line profiles show the same three strong components ordered at the same relative velocities within the errors. The intensity ratio of the three components is steeper in H$\alpha$ than in H$\beta$ (Figs. 3, 4). The Balmer decrements of the individual line segments are listed in Table 2 (Sect. 3.2).

### *3.2. Light curves of H$\alpha$ emission line segments*

The light curves of the integrated H$\alpha$ line as well as of the continuum flux at 6310 Å were given in Paper I for the epochs from Jan. until June 1990. The variability pattern of both light curves is very similar. Strong variations up to 25 per cent within 5 days were to be seen.

Here, we discuss the variations of individual segments of the broad H$\alpha$ line profile. We divided the broad H$\alpha$ profile in 7 segments with respect to the shape of the rms profile (Fig.3) and with respect to the difference profiles (Fig.2). The core segment contains the central component only; the inner wing components include the strong line components at ($v_{rel}$ = $\pm$1000 km s$^{-1}$) and the remaining parts of the line wings have been divided in two further segments. The extent of these segments is given in Table 2. The intensities of the line segments and their variations are listed in Table 1. The individual light curves of the line core, of the integrated inner and middle wings as well as of the outer line wings are displayed in Fig. 5.

**Table 2.** Extension of individual H$\alpha$ segments, maximum to minimum H$\alpha$ flux ratio and the Balmer decrement of the rms profile segments.

| segment | $v_{rel}$ [km s$^{-1}$] | max/min flux | rms: H$\alpha$/H$\beta$ |
|---|---|---|---|
| outer blue wing | $-5000 \ldots -2500$ | 1.50 | 5.8 |
| middle blue wing | $-2500 \ldots -1500$ | 1.56 | 9.5 |
| inner blue wing | $-1500 \ldots -500$ | 1.62 | 10.7 |
| core | $-500 \ldots +500$ | 1.61 | 13.5 |
| inner red wing | $+500 \ldots +1500$ | 1.85 | 13.4 |
| middle red wing | $+1500 \ldots +2500$ | 1.95 | 7.4 |
| outer red wing | $+2500 \ldots +5000$ | 1.55 | 4.2 |

At a first glance the light curves of the H$\alpha$ core and of the continuum flux (Paper I) can be divided in two sections with respect to its pattern — a decreasing phase (JD...7891 until JD...7968) and an outburst (JD...7968 until JD...8049). Within the decreasing period the integrated H$\alpha$ flux dropped by nearly 30 per cent and recovered to the former flux level within 10 days. But on closer inspection one can see systematic differences in the light curves of the inner and outer line segments. For example, the minimum state at JD...7968 is more pronounced in the light curves of the inner line segments with respect to the secondary minimum at JD...7916. This holds not for the outer line segments. On the other hand there are systematic differences between the blue and red line wings. Sometimes the line wings vary parallel with respect to the line center but at some epochs there are strong variations. To show this in more detail we plotted in Fig. 6 the intensity ratio of the blue to the red H$\alpha$ wing as a function of integrated line intensity. One can see

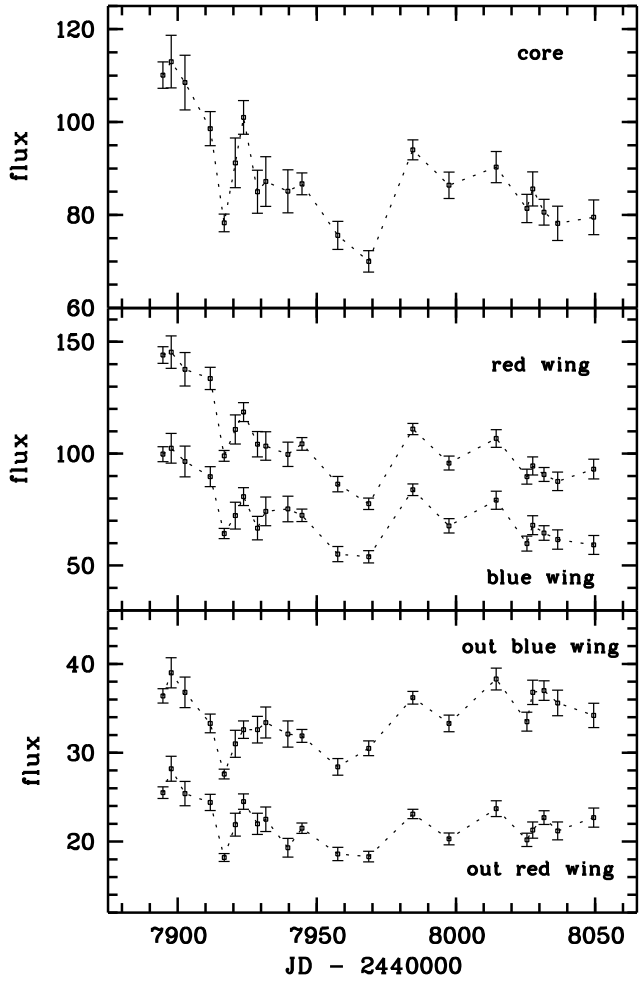


**Fig. 5.** Light curves of the H$\alpha$ line core, of the integrated inner and middle wings (blue wing shifted by -30 flux units) as well as of the outer wings (blue wing shifted by 5 flux units). The points are connected by a dotted line to aid the eye.

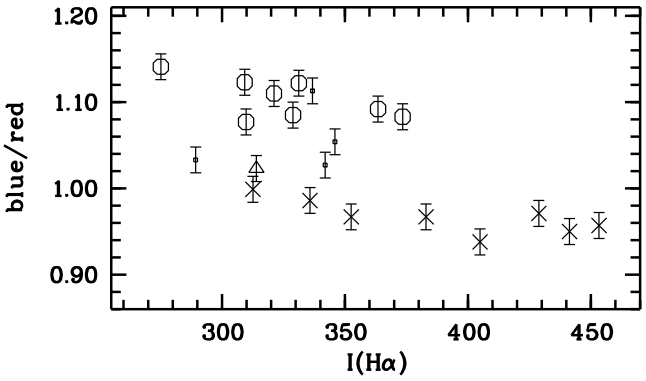


**Fig. 6.** Intensity ratio of the blue (-5000 ... -500 km s$^{-1}$) to the red (500 ... 5000 km s$^{-1}$) H$\alpha$ wing as function of integrated line intensity. Data points of the first half of the first outburst (JD7894 - JD7928): crosses; second half of the first outburst (JD7931 - JD7957): dots; second outburst (JD 7968 - JD8036): open circles; last epoch of campaign (JD8049): triangle.

systematic differences in the ratio of the blue to red H$\alpha$ wings for different epochs.

### *3.3. Line profile variations*

For a detailed study of the H$\alpha$ profile variations we computed difference profiles with respect to the minimum state at JD...7968 as well as difference profiles of subsequent observing epochs. In Fig. 2 the difference profiles with respect to the minimum state were plotted. The top panel shows spectra taken during the strong intensity drop (decreasing phase) at JD..7897, 7902, 7911, 7916; the upper middle panel presents the increasing phase at JD..7916,7920,7923; the lower middle panel shows the second half of first outburst at JD..7923,7928,7931,7957; in the bottom panel the second outburst at JD..7984,8014,8025,8036 is given. Not all H$\alpha$ difference spectra are shown to avoid confusion in the figures. The three strong line components that were seen in the H$\alpha$ rms profiles can be recognized in all these difference profiles too, except in the spectrum taken at JD...7957 near the minimum state where only a weak central component is visible. The line components are ordered at the following relative velocities with respect to the narrow H$\alpha$ component: a red component at $v_{rel}$ = +1000 ± 50 km s$^{-1}$, a central component at $v_{rel}$ = +80 ± 50 km s$^{-1}$, and a blue component at $v_{rel}$ = −1000 ± 100 km s$^{-1}$. For some times an additional blue component can be detected at $v_{rel}$ = −1300 ± 100 km s$^{-1}$.

During the second outburst (JD..7984 — 8036) two weak outer line components at $v_{rel}$ = 2700 ± 100 km s$^{-1}$ and at $v_{rel}$ = −3000 ± 100 km s$^{-1}$ can be seen in the difference spectra (Fig. 2, bottom panel). The inner blue and red H$\alpha$ components in the difference profiles are ordered at similar but not identical relative velocities. They vary nearly simultaneously and they have similar amplitudes. But the core component as well as the outer line wing components have different amplitudes (e.g. during the period: JD...7916 — 7923). This could be seen in the light curves (Fig.5) too. At certain epochs one can observe variations of individual components only: e.g. the variation of a blue component at $v_{rel}$ = −1300 km s$^{-1}$ from JD..7928 to JD..7931 while other components remained constant (Fig. 2, middle panel). Likewise we could detect variations of the central component or of individual other line components by comparing observations taken within of few days. These short term variations of individual components are better recognizable in the difference profiles of subsequent epochs (Fig. 7, upper panels). The variations of more than one component are plotted in the difference spectra of longer time intervals (Fig. 7, lower panels).

The relative velocities of the individual components remained constant in velocity space during our observing period of six months. The shape of the central component is distinct with respect to the outer components. The profile is very narrow at the top and broadens until ∼ 6000 km s$^{-1}$ (FWZI) at the bottom. (Fig. 7, top panel). The outer line components (e.g. at

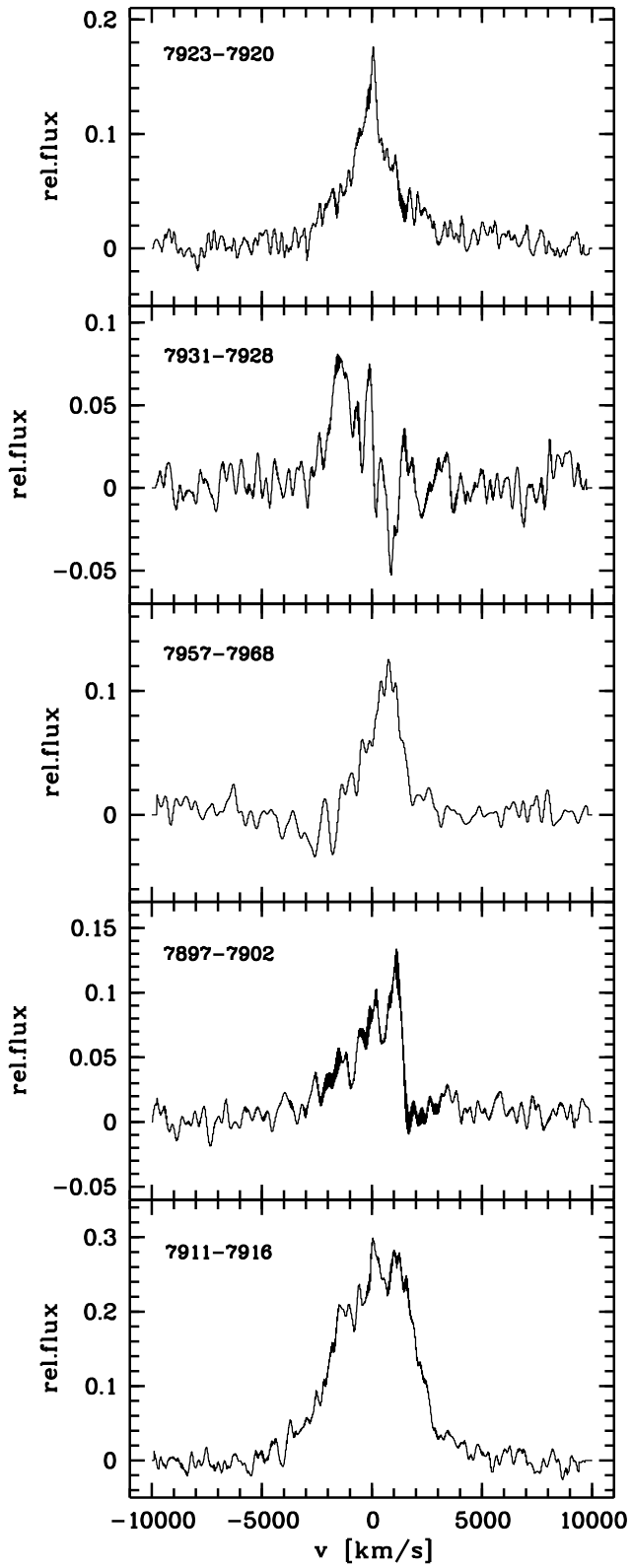


**Fig. 7.** Hα difference profiles of subsequent epochs.

**Table 3.** Results of the CCF analysis of the Hα emission line sections vs. the optical continuum light curve in units of days. The uncertainty of the delay given by $\sigma_{GP}$ was estimated by using the equation (4) in Gaskell & Peterson (1987).

| section | $\tau_{cent}$ | $\sigma_{GP}$ | $CCF_{max}$ | FWHM |
|---|---|---|---|---|
| outer blue wing | -0.4 | 1.2 | 0.55 | 11.4 |
| middle blue wing | 3.0 | 1.7 | 0.84 | 22.0 |
| inner blue wing | 4.0 | 1.9 | 0.85 | 24.7 |
| line core | 2.8 | 2.0 | 0.83 | 25.6 |
| inner red wing | 4.9 | 2.8 | 0.83 | 36.1 |
| middle red wing | 4.6 | 2.1 | 0.88 | 27.7 |
| outer red wing | 0.2 | 1.4 | 0.84 | 18.4 |

JD...7916, JD...7957) have steeper profiles with typical FWZIs of a few 1000 km $s^{-1}$ only.

### *3.4. CCF analysis of Hα line segments*

The light curve of the integrated Hα line shows the same overall pattern as the continuum light curve. In Paper I we cross-correlated these two light curves using a method described by Gaskell & Peterson (1987) and White & Peterson (1994). We averaged the centroids of the ICCFs that were calculated for fractions of the peak ranging from 30 per cent to 85 per cent of the maximum value of the cross-correlation function. In this way we determined a mean value of the centroid $\tau_{cent}$ of the cross-correlation function (ICCF). We calculated a delay of $\tau_{cent}$ = 3.8 ± 2.0 days of the integrated Hα line with respect to the optical continuum. This delay can be taken as a measure of the mean distance of the line emitting region relative to the central source under the assumption that the optical continuum light curve represents the ionizing radiation.

In Fig.5 and Table 1 the light curves of individual Hα segments are given. As had been said before there are differences in the light curves of individual line segments. Now we correlated the light curves of all individual Hα segments (Table 1) with the optical continuum light curve (Paper I). The different line profile segments represent different velocity components in the BLR of NGC 4593. The resulting delays of the individual profile sections we determined from the mean centroids $\tau_{cent}$ of the ICCFs (see above) are given in Table 3.

The delays of the Hα segments are plotted in Fig. 8 as function of location in velocity space. The error bars of $\tau_{cent}$ were calculated using equation (4) of Gaskell & Peterson (1987). We got the following trends. The outer Hα wings show no detectable delay with respect to the optical continuum. Therefore, the line emitting material that represents the high velocity part of the velocity field - i.e. the outer wings of the profile - should originate very close to the ionizing continuum source or the gas is located close to the line of sight. The inner parts of the line profile are characterized by a similar delay. These individual Hα sections react nearly simultaneously to continuum variations. There might be a larger delay of the inner red wing with respect to the inner blue wing.

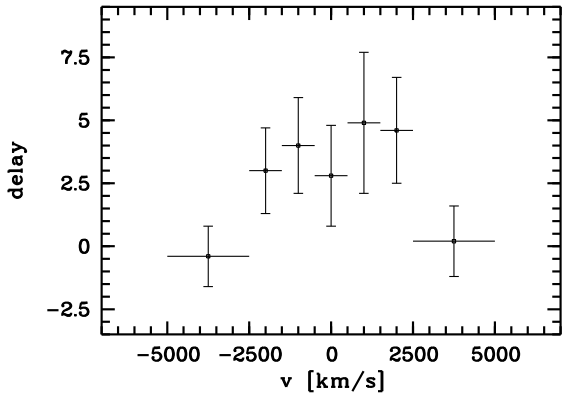


**Fig. 8.** Delays (in units of days) of individual segments (outer blue wing, middle blue wing, inner blue wing,core, inner red wing, middle red wing,outer red wing) of the H$\alpha$ line profile with respect to the optical continuum at $\lambda$ = 6310Å.

In Fig. 9 the ICCFs of the individual parts of the line profile are displayed. The ICCFs of the inner line wings and of the middle line wings were combined. The ICCFs of the outer wings of the line profile are very similar as well as the ICCFs of the inner parts of the H$\alpha$ profile. But the ICCFs of the inner sections show an additional prominent strong wing at positive delays in contrast to the ICCFs of the outer wings. This causes the shift of the ICCFs of the inner line segments to delays greater than zero.

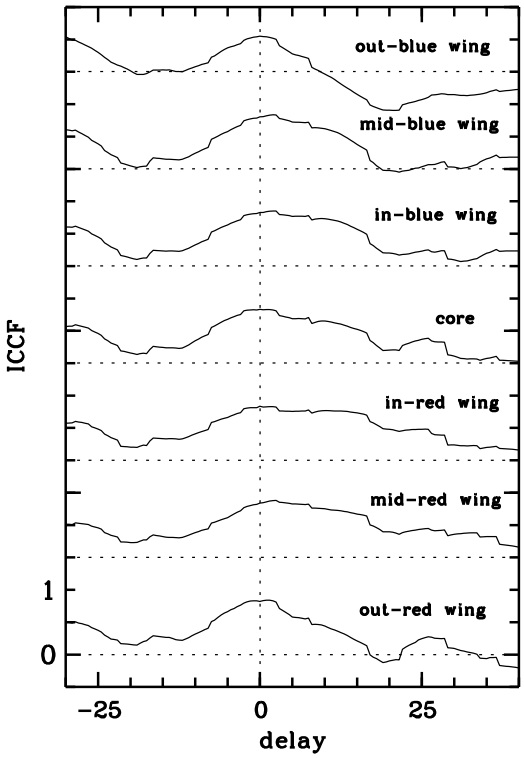


**Fig. 9.** ICCFs of H$\alpha$ line segments. The ICCFs are shifted vertically. The delay is plotted in units of days.

## 4. Discussion

The nearby Seyfert galaxy NGC 4593 varied strongly in the past. We observed variations in the optical continuum, in the broad emission line intensities and in the line profiles on very short timescales of the order of a few days only. Due to the relative low absolute magnitude of the host galaxy variations of smaller intrinsic intensity can be detected more easily in comparison to other bright AGNs. The amplitudes of the optical continuum intensities at 6310 Å and of the total H$\alpha$ flux were of the same order during our variability campaign in 1990. Within a period of 60 days we detected variations of 68 per cent in the continuum and of 53 per cent in the integrated H$\alpha$ flux. These data represent lower limits only due to the contributions of the nonvariable host galaxy components in the continuum and of the narrow line components in the H$\alpha$ flux (see Paper I). The H$\beta$ line showed even more violent variations of the order of 100 per cent during the campaign.

For a detailed study of the profile variations we calculated the mean and rms profiles of H$\alpha$ and H$\beta$ (Figs. 3, 4). Not only the widths but also the shapes of these profiles are different. The intensity distribution in the rms line profile is a criterion for the variable portion in the profile. A comparison of the rms profiles with the mean profiles indicates that the line variations are more concentrated to the inner part of the profile. This is comparable to the variations in Mkn 590 (Peterson et al. 1993). The rms profiles in NGC 4593 are not symmetric with respect to $v_{rel}$ = 0 km s$^{-1}$. The outer blue wings $v_{rel} \geq -3000$ km s$^{-1}$ are more intense than the outer red wings. This might be explained by a radial velocity component in the BLR or by unequal line absorption. A blue asymmetry in the outer wings of the Balmer rms profiles has been detected in NGC 5548, too (Kollatschny & Dietrich 1996). The rms profiles and the difference profiles of H$\alpha$ and H$\beta$ are structured. They consist of three to five strong components only (Figs. 3,4). The line profile components originate more or less pairwise and they have similar relative velocities with respect to $v_{rel}$ = 0 km s$^{-1}$ apart from the central component. But neither their relative velocities nor the intensities of the pairwise components are exactly the same. The relative velocities of the line components remained constant during the observing period. The strongest components at $v_{rel} = 1000, 0, -1000$ km s$^{-1}$ can be seen in the H$\alpha$ as well as in the H$\beta$ rms-profiles. They originate at the same velocities. The component at $v_{rel}$ = 1000 km s$^{-1}$ is to be seen in H$\alpha$ as well as in H$\beta$; therefore this component is not an artefact in the H$\alpha$ profile due to a residual of the [NII]$\lambda$ 6583 line. But the relative intensities of the line components are different in H$\alpha$ and H$\beta$. The result that the Balmer decrement of line components is different (Table 2) is an indication that the components originate in distinct regions under different physical conditions or that the reddening is different. The Balmer decrement increases from the outer wings to the line core. This might be explained by radiative transfer effects or by the increasing of dust obscuration in the inner segments of the line profiles. This means that

the obscuration by dust or the dust content is more important in the outer BLR in comparison to the inner BLR under the assumption that the inner line profile segments originate in the outer region of the BLR.

The pattern of the integrated H$\alpha$ line variation follows closely but not exactly that of the optical continuum. The individual components of the emission line varied with different amplitudes (Table 2). At the beginning of the second outburst (JD...7968) a red line component at $v_{rel}$ = 500 km s$^{-1}$ (see Fig. 7 middle panel: JD...7957 - JD...7968) decreased. The decreasing of this component is responsible for the decreasing of the red wing light curve (Fig. 5) from JD...7957 until JD...7968 while the blue wing intensity remained constant. In Fig. 6 it is shown that the blue to red line asymmetry changed from 1.03 to 1.14 for those two epochs having the lowest integrated H$\alpha$ intensity. During the following period (JD...7968 — JD...8086) (Fig. 6, open circles) the line asymmetry remained constant independent of the integrated intensity. Those components which are arranged symmetrically with respect to $v_{rel}$ = 0 km s$^{-1}$ show more or less the same variations (Fig. 2). These observations can be explained by a variable central ionizing source having a biconical structure or by a bidimensional distribution of the ionized clouds. The asymmetric changes (Fig. 6) might be explained by the existence or absence of individual line components. Therefore, the distribution of the line emitting clouds can not be homogeneous. Only a limited number of clouds or cloud complexes must be responsible for the emission line flux since individual substructures can be detected in the profiles (cf. Figs. 2,3,7).

On the other hand the variability amplitude is stronger in the red H$\alpha$ wing, especially in the inner red wing, in comparison to the blue wing (Table 2, Fig. 5). Our finding that the variations of the inner H$\alpha$ wings are more violent than those of the outer wings is distinct to CIV$\lambda$1548 line variations reported by Santos-Lleó et al. (1995). However, their IUE observations (1981-1987) were carried out some years earlier. And one has to consider that the pattern of line profile variations can be different from line to line and from outburst to outburst. We detected independent variations in distinct lines in NGC 5548 during the same outburst (Kollatschny & Dietrich 1996).

The central Balmer component has a different profile shape with respect to the outer components (cf. Fig. 7). Furthermore, this component does not vary with the same amplitude (Fig. 5). Therefore, the line components originate under different physical conditions. This result is in agreement with an independent observation of Wills et al. (1993). They made a statistical investigation of the CIV$\lambda$1548 broad emission line profiles in a sample of more than hundred QSOs. In this completely alternative approach they found that the broad emission lines can be described by two components: a core component with a characteristic width of 2000 km s$^{-1}$ FWHM and a broad component.

The cross-correlation functions of the integrated H$\alpha$ emission line intensities and of line segments in NGC 4593 indicate that they originate very close to the central region at a distance of less than five light days. Therefore, this is is one of the smallest BLR sizes known today in Seyfert galaxies. Koratkar & Gaskell (1991) and Santos-Lleó et al. (1995) got from their optical and UV line variations upper limits of a few days too. The ICCFs of the outer H$\alpha$ wings point to even shorter delays with respect to the optical continuum: less than two days. This is the shortest delay found so far in optical line variability campaigns of AGNs. The fact that the line wings respond faster than the line cores was found in NGC 5548, too (Korista et al. 1995, Kollatschny & Dietrich 1996). Therefore, those emission line clouds having the highest relative velocities originate closest to the central source. The cross-correlations of the inner wings and of the line core show that the variations are simultaneously within the uncertainties. Therefore, the BLR seems not to be dominated by radial motions.

The central component in NGC4593 is redshifted by $v_{rel}$ = 110 $\pm$ 30 km s$^{-1}$ with respect to the narrow line components. We measured such a shift in the rms spectrum of H$\alpha$ as well as in the individual H$\alpha$ difference spectra. The H$\beta$ rms spectrum shows a redshift of the same order. The observed redshift might be interpreted as gravitational redshift. One can make a rough estimation of the mass of the central object (e.g. Zheng & Sulentic 1990) assuming the observed redshift of $v_{rel}$ = 100 km s$^{-1}$ can be attributed to the gravitation of a massive central object and the H$\alpha$ core component originates at a distance of 4 lt-days from the center:

$$M \leq c^2 G^{-1} R \Delta z$$

Using this formula we determined the mass of the central object to:

$$M \leq 2.3\ 10^7 M_\odot$$

Furthermore, one can estimate the central mass in AGNs in another way by measuring the width of the broad emission line profiles (FWHM) ( under the assumption that the gas dynamics are dominated by the central massive object ) and by determing the distance of the emission line clouds to the center (e.g. Koratkar & Gaskell 1991):

$$M = \frac{3}{2} v^2 G^{-1} R$$

We get a central mass of:

$$M = 1.4\ 10^7 M_\odot$$

assuming the characteristic velocity of the H$\alpha$ emission line region is given by their FWHM (3500 km s$^{-1}$) and the characteristic radius is given by the cross correlation function (4 lt-days). Both independent estimations result in a central mass of the order of $10^7 M_\odot$ in NGC 4593.

## 5. Summary

Strong variations in the Balmer line profiles of NGC 4593 have been detected. The emission lines can be described by three to five strong components only: a core component and outer components located nearly symmetrically with respect to $v_{rel}$ = 0

km $s^{-1}$. These components can be recognized in the rms profiles and in the difference spectra. The individual components varied in different ways. We observed variations of individual line components on time scales of a few days only. The line segments originate in different regions of the BLR under different physical conditions considering their variability amplitudes, their Balmer decrements and their time delays with respect to the continuum. The outer line wings respond within of two days to continuum variations. A dominant radial velocity component can be excluded in the BLR of NGC 4593.

*Acknowledgements.* This work has been supported by DFG grant Ko 857/13-1 (Universitäts-Sternwarte Göttingen) and SFB328D (Landessternwarte Heidelberg). We thank K. Jäger for useful comments.

## References

Blandford R.D. & McKee C.F., 1982, ApJ, 255, 419
Blumenthal G.R. & Mathews W.G., 1975, ApJ, 198, 517
Carroll T.J. & Kwan J., 1985, ApJ, 288, 73
Dietrich M., Kollatschny W., Alloin D., et al., 1994, A&A , 284, 33 (Paper I)
Gaskell C.M. & Peterson B.M., 1987, ApJS, 65, 1
Kollatschny W. & Dietrich M., 1993, Astrophys. Sp. Science, 205, 179
Kollatschny W. & Fricke K.J., 1989, A&A ,219, 34
Kollatschny W. & Dietrich M., 1996, A&A in press
Koratkar A. & Gaskell M., 1991, ApJL, 370, L61
Korista K.T., Alloin D., Barr P., et al., 1995, ApJS, 97, 285
Peterson B.M., 1987, ApJ, 312, 79
Peterson B.M., Ali B., Horne K., et al., 1993, ApJ, 402, 469
Robinson A., 1995, in 'Reverberation Mapping of the Broad-Line Region of AGN', A.S.P.Conference Series Vol.69, eds. K. Horne, B.M. Peterson, & P.M. Gondhalekar, p.147
Robinson A. & Pérez E., 1990, MNRAS, 244, 138
Santos-Lleó M., Clavel J., Barr P., Glass I.S., Pelat D., Peterson B.M., & Reichert G., 1994, MNRAS, 270, 580
Santos-Lleó M., Clavel J., Barr P., et al., 1995, MNRAS, 274, 1
Stirpe G.M., De Bruyn A.G., & van Groningen E., 1988, A&A, 200, 9
Wanders I. & Peterson B.M., 1996, ApJ in press
Welsh W.F. & Horne K., 1991, ApJ, 379, 586
White R.J. & Peterson B.M., 1994, PASP, 106, 879
Wills B.J., Brotherton M.S., Fang, D., et al., 1993, ApJ, 415, 563
Zheng W. & Sulentic, J., 1990, ApJ, 350, 512
Zheng W., Pérez E., Grandi S.A., & Penston M.V., 1995, AJ, 109, 2355

This article was processed by the author using Springer-Verlag LaTeX A&A style file *L-AA* version 3.